RSC Advances

PAPER

View Article Online
View Journal | View Issue

Cite this: *RSC Adv.*, 2025, **15**, 388

AgNPs/CuNPs/Bragg-PSi substrate subjected to thermal annealing in high-sensitivity detection on crystal violets and diphenyl phthalate†

Bowen Sun, Peng Li,* Shuguo Yu, Xiaohui Huang and Liangjun Ma

This study has successfully prepared three kinds of surface enhanced raman scattering (SERS) substrates, namely AgNP/CuNPs/Bragg-PSi (porous silicon, PSi), AgNPs/CuNPs/PSi and AuNPs/CuNPs/Bragg-PSi by use of an anode electrochemical etching method and a dip plating method. Results show that: the AgNPs/CuNPs/Bragg-PSi substrate has optimal SERS performance and is capable of detecting the Raman spectrum (R^2 = 0.9315) of a 10^{-5} M–10^{-11} M crystal violet (CV) solution. By virtue of optimizing the concentration of copper nitrate for soaking the AgNPs/CuNPs/Bragg-PSi substrate and the annealing temperature for the AgNPs/CuNPs/Bragg-PSi substrate, this study has explored the influence of different preparation conditions on the performances of the substrate. Results show that: the optimal soaking concentration of the copper nitrate solution is 0.75 M, and the AgNPs/CuNPs/Bragg-PSi substrate annealed at 180 °C shows a more uniform microscopic structure and a stronger surface-enhanced effect. Finally, the annealed AgNPs/CuNPs/Bragg-PSi substrate is capable of realizing the high-sensitivity detection (R^2 = 0.9898) on diphenyl phthalate within a concentration range of 10^{-3} M to 10^{-9} M. The AgNPs/CuNPs/Bragg-PSi substrate has the advantages of easiness and convenience in preparation, low cost, high sensitivity and the like, thus providing a broad prospect for application of SERS technology in the fields of chemical analysis and biological analysis and laying a foundation for developing more sensitive and reliable detection methods.

Received 29th June 2024
Accepted 22nd November 2024

DOI: 10.1039/d4ra04726e

rsc.li/rsc-advances

1 Introduction

As one of phthalic acid ester (PAEs) plasticizers, diphenyl phthalate (DPHP) is a white crystalline solid insoluble in water and has wide application value in teh plastics industry[1,2] and synthesis of polymer materials.[3,4] However, studies show that DPHP may has adverse effects on the human reproductive system,[5] endocrine system[6] and nervous system,[7,8] therefore rapid and accurate detection on DPHP is quite important.[9,10] At present, common detection methods include high performance liquid chromatography (HPLC),[11,12] gas chromatography-mass spectrography (GC-MS),[13] enzyme-linked immunosorbent assay[14,15] and the like, however these methods have the problems of complex sample pretreatment, long detection time, relatively expensive detection equipment and the like. Therefore, seeking a more efficient, rapider and low-cost method has important significance in guaranteeing the product quality and the human health.

In recent years, the Surface Enhanced Raman Scattering (SERS) technology has attracted wide attention due to a series of advantages such as high detection sensitivity, high resolution and strong stability.[16] The SERS technology can realize the rapid detection on trace analytes by enhancing the Raman vibration signal of molecules,[17] and it shows great application potential in biomedicine, environmental monitoring, food safety and other fields.[18–21]

In preparation of the SERS substrate, the Bragg-PSi substrate has excellent optical properties and structure stability.[22] Bragg-PSi was modified with metal nanoparticles,[23] thus the SERS signal was significantly enhanced by use of the localized surface plasmon resonance (LSPR) effect of metal nanoparticles.[24] Meanwhile, thermal annealing is a common post-processing method.[25] By controlling the annealing temperature and time, the morphology and distribution of nanoparticles can be effectively regulated, thus significantly improving the strength and stability of SERS signals.

In this study, the AgNPs/CuNPs/Bragg-PSi substrate optimized by thermal annealing was used to achieve high-sensitivity detection on CV and DPHP,[26] thus providing a new idea and method for the application of the SERS technology in environmental analysis and biological detection, and exploring its practical application potential in high-sensitivity analysis.

School of Physical Science and Technology, Xinjiang University, 666 Shengli Road, Urumqi 830046, China. E-mail: lipeng19810701@163.com

† Electronic supplementary information (ESI) available. See DOI: https://doi.org/10.1039/d4ra04726e

2 Experimentation part

2.1 Materials

$AgNO_3$ (99.8%), $Cu(NO_3)_2 \cdot 3H_2O$, chloroauric acid, acetone, hydrofluoric acid and alcohol were purchased from Sinopharm Chemical Reagent Co., Ltd. The CV and DPHP were purchased from Shanghai Aladdin Biochemical Technology Co., Ltd, and monocrystalline silicon was purchased from Tianjin Institute of Conductor Technology (Tianjin, China). All chemicals were of analytical grade and used without further purification.

2.2 Preparation of SERS substrate

2.2.1 Preparation of monolayer and multilayer porous silicon. In the experiment, p-type boron-doped monocrystalline silicon (crystal orientation <100>, resistivity 0.03–0.06 Ω·cm, thickness 400 + 10 μm) was adopted, and the experiment steps were as follows: cutting silicon wafers into squares of 2 cm × 2 cm, putting the silicon wafers into beakers, adding acetone and ethanol respectively, and cleaning the silicon wafers in an ultrasonic cleaning machine for 15 min so as to ensure the surface cleanliness and smoothness of the silicon wafers; preparing an etching solution ($HF : C_2H_5OH = 1 : 1$), shaking the etching solution evenly and then standing the etching solution; fixing the cleaned silicon wafers into a single-tank anode electrochemical etching device, pouring the etching solution into the etching tank in which the silicon wafer was fixed, and preparing a single-layer porous silicon structure by setting the current density to 80 mA cm^{-2} and the etching time to 16 s through the Labview procedure (National Instruments, Ltd, USA); setting the current density of a layer with high refractive index and a layer with low refractive index to 65 mA cm^{-2} and 115 mA cm^{-2} respectively and the etching time to 1.2 s and 1 s respectively, and repeating 12 cycles so as to prepare a Bragg-PSi structure; taking out the prepared porous silicon substrate from the etching tank; and cleaning the porous silicon substrate with ethanol and deionized water respectively for later use.

2.2.2 Binding of metal nanoparticles onto porous silicon substrate. In the experiment, a dip plating method was adopted for fixing metal nanoparticles to the surface of porous silicon, and the specific operations were as follows: respectively preparing $Cu(NO_3)_2$ solutions with concentrations of 0.1 M, 0.25 M, 0.5 M, 0.75 M and 1 M, a 0.01 M $AgNO_3$ solution and a 0.01 M $HAuCl_4$ solution; soaking the prepared PSi substrate with the 0.1 M $Cu(NO_3)_2$ solution for 1 min, rinsing the PSi substrate with deionized water, then drying the PSi substrate, soaking the PSi substrate in the 0.01 M $AgNO_3$ solution for 50 s, then taking out the PSi substrate, rinsing and drying the PSi substrate, thus preparing a CuNPs/AgNPs/PSi substrate; based on the same method, sequentially soaking a Bragg-PSi substrate with the 0.1 M $Cu(NO_3)_2$ solution for 1 min and with the 0.01 M $HAuCl_4$ solution for 50 s, thus preparing a CuNPs/AuNPs/Bragg-PSi substrate; and then sequentially soaking a Bragg-PSi substrate with the 0.1 M $Cu(NO_3)_2$ solution for 1 min and with the 0.01 M $AgNO_3$ solution for 50 s, thus preparing a CuNPs/AgNPs/Bragg-PSi substrate. Single crystal silicon undergoes etching with HF and ethanol, resulting in the formation of porous silicon and the production of a significant

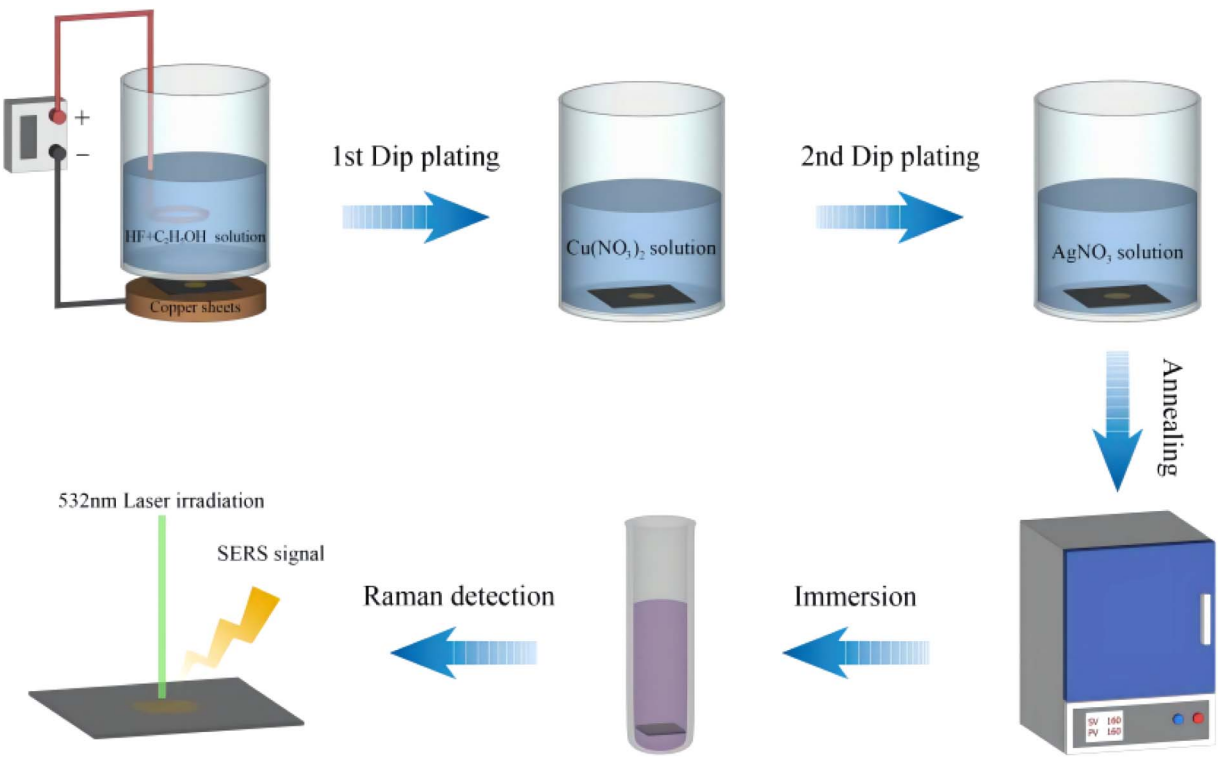

Fig. 1 The preparation and detection process of the SERS substrate.

number of silicon–hydrogen bonds on the surface. These silicon–hydrogen bonds possess reducing properties, which are harnessed to reduce CuNPs from a $Cu(NO_3)_2$ solution onto the surface of the porous silicon. The preparation method for AgNPs involves a displacement reaction, and it also utilizes the remaining silicon–hydrogen bonds on the surface of the porous silicon to reduce AgNPs.

Single crystal silicon undergoes etching with hydrofluoric acid and ethanol, resulting in the formation of porous silicon and the production of a significant number of silicon–hydrogen bonds on the surface. These silicon–hydrogen bonds possess reducing properties, which are harnessed to reduce CuNPs from a $Cu(NO_3)_2$ solution onto the surface of the porous silicon. The preparation method for AgNPs involves a displacement reaction, and it also utilizes the remaining silicon–hydrogen bonds on the surface of the porous silicon to reduce AgNPs.

2.2.3 Raman spectrum detection. A confocal Raman spectrometer (BWS465-532S, BWTEK) was used to test the to-be-tested substance. The operations were as follows: under the conditions of a 532 nm laser, 30% laser power, 10 s integration time, 3 average times and a 20× objective lens, measuring each sample of same concentration at different sites for at least 5 times, and then averaging, thus obtaining spectral data; and before detection, soaking the substrate with a to-be-tested solution for 3 h, then taking out the substrate, and naturally drying the substrate at a room temperature for test, wherein the whole experiment process is as shown in Fig. 1. In the process of Raman detection, the metal nanoparticles have greatly inhibited the fluorescence phenomenon of the to-be-tested substance, but the intensity shift may still occurred due to some environmental influences, resulting in baseline fluctuation. Therefore, the baseline calibration in BWSpec was uniformly used to adjust the baseline of the measured spectral information to the same level, thereby correcting the vertical deviation error caused by other factors without affecting the relative relationship between Raman peaks.

3 Results and discussion

3.1 Morphological characteristics analysis of SERS substrate

Fig. 2(a) is a surface scanning electron microscope image of the AgNPs/CuNPs/PSi substrate. The pore size of PSi is about 25 nm, and the size of AgNPs is about 50–100 nm. Although the etching time for preparing the single-layer porous silicon in the three substrates is the shortest, there are still enough Si–H bonds for reducing metal nanoparticles. Fig. 2(b) shows the AgNPs/CuNPs/Bragg-PSi substrate, an AgNPs agglomeration phenomenon occurs, thus its uniformity is worse than that of the AgNPs/CuNPs/PSi substrate; the reason is that this substrate is of a multi-layer porous silicon structure arranged in 12 cycles, the etching time is longer, more Si–H bonds are generated on the surface, and more Cu nanoparticles are reduced, so that an agglomeration phenomenon occurs during secondary reduction of Ag nanoparticles, therefore the uniformity is lower than that of the first structure. Fig. 2(c) shows the AuNPs/CuNPs/Bragg-PSi substrate, the size of a single Au nanoparticle is about 50 nm, but it has a relatively uniform morphology size and arrangement structure. The contrast aims to show that by virtue of SEM images, it can be clearly observed that the porous silicon substrate prepared by the anode electrochemical etching method is successfully compounded with metal nanoparticles.

3.2 Characterization and analysis of SERS substrate

The sensitivity of the prepared AgNPs/CuNPs/PSi substrate, the prepared AuNPs/CuNPs/Bragg-PSi substrate and the prepared AgNPs/CuNPs/Bragg-PSi substrate is detected by using CV as probe molecules. The Raman spectrum of CV usually covers the wave number range from 400 cm^{-1} to 1800 cm^{-1}, wherein the Raman peak of CV at 1617 cm^{-1} is the most significant characteristic peak, which represents the Raman scattering of benzene rings in CV molecules. Therefore, we choose the peak value at 1617 cm^{-1} as comparative analysis. The following information can be obtained by comparing the spectra: by comparing Fig. 3(a) with Fig. 3(c), the results show that the detection limit of detecting CV by use of the single-layer porous silicon substrate is 10^{-8} M, while the detection limit under a Bragg-PSi structure can reach 10^{-11} M. It can be found that the combination of AgNPs and CuNPs on the porous silicon substrate has a good performance in amplifying the Raman signal of a substance,[27] which is due to the large specific surface area of the porous silicon structure, thus more SERS active sites can be provided. However, on the single-layer porous silicon substrate and the Bragg-PSi substrate, the attenuation degree of the peak intensity of the Raman signal strength of the single-

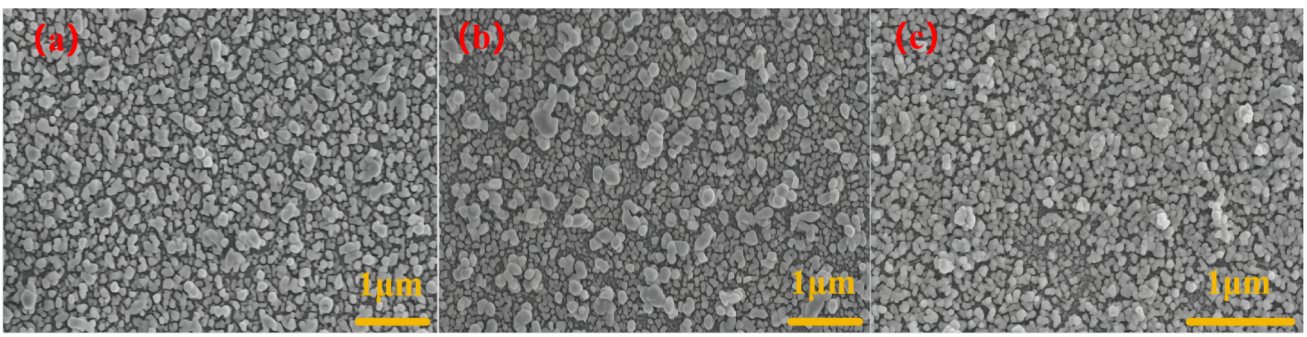

Fig. 2 (a) AgNPs/CuNPs/PSi; (b) AgNPs/CuNPs/Bragg-PSi; (c) AuNPs/CuNPs/Bragg-PSi.

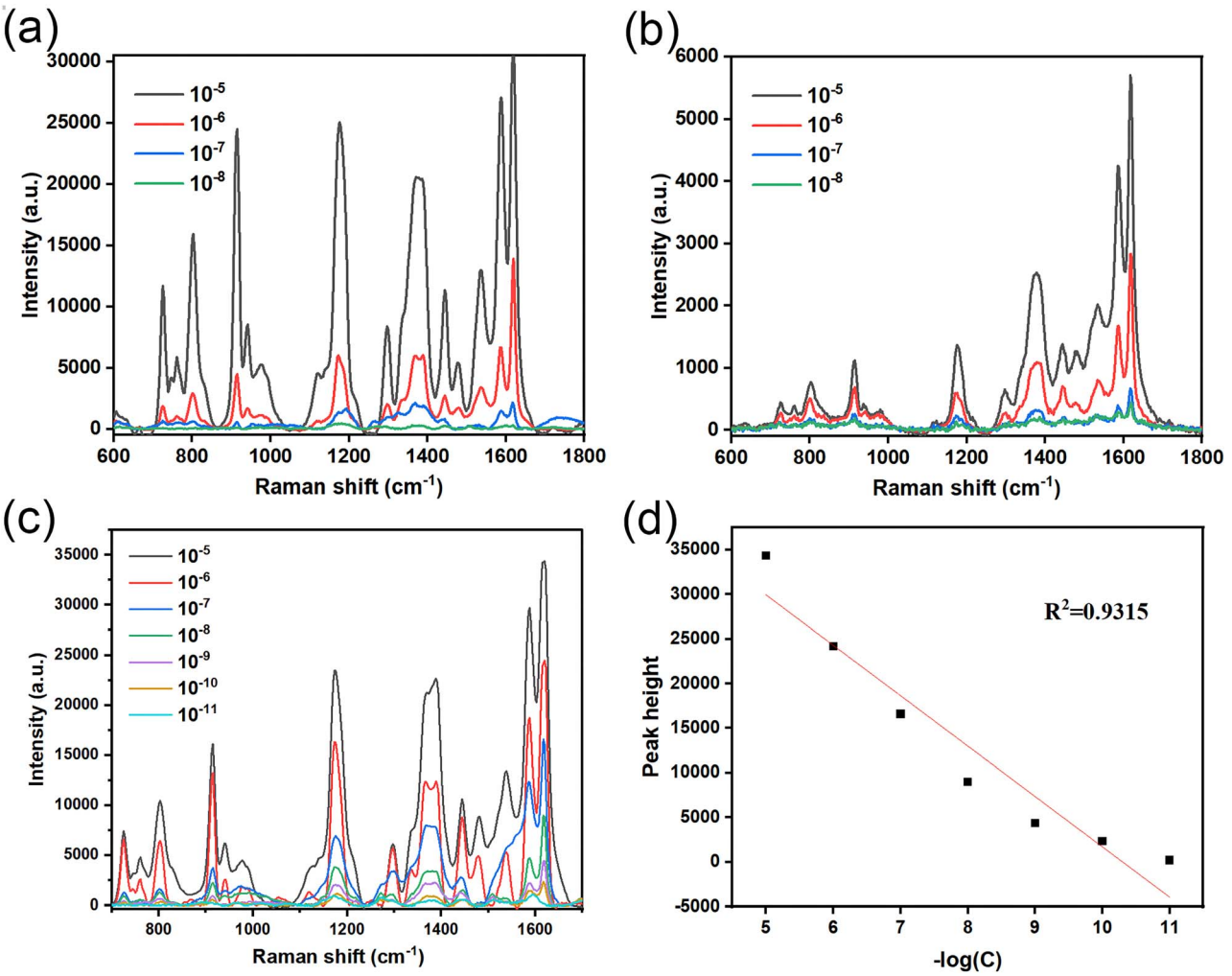

Fig. 3 (a)–(c) respectively show the detection on different concentrations of CV solutions by use of the AgNPs/CuNPs/PSi substrate, the AuNPs/CuNPs/Bragg-PSi substrate and the AgNPs/CuNPs/Bragg-PSi substrate. (d) Shows the linear fitting between the negative logarithm of the AgNPs/CuNPs/Bragg-PSi substrate for the CV solution concentration and the linear fitting degree of its Raman peak intensity at 1617 cm^{-1}.

layer porous silicon substrate is much greater than that of the Bragg structure along with the decrease of substance concentration. This is because the Bragg-PSi substrate has excellent optical properties. Compared with the single-layer porous silicon substrate, the Bragg-PSi substrate has more pores and surface areas in the same volume, and the Bragg-PSi substrate has the characteristics of Bragg diffraction and is capable of realizing high reflection of lights with specific wavelengths, which means that the SERS active sites excited on this substrate can better use the energy of the incident light, thereby increasing the strength of the SERS signals. However, due to the low stability of Ag nanoparticles, Au nanoparticles are introduced to prepare the above AuNPs/CuNPs/Bragg-PSi substrate detection CV solution as shown in Fig. 3(b). Since the obtained Raman signal is weak, we increase the power of the laser to 80%, thus obtaining that the detection limit of the AuNPs/CuNPs/Bragg-PSi substrate for CV is 10^{-8} M. It can be found that when AuNPs/CuNPs/Bragg-PSi is used as the SERS substrate, the cost is high and the performance is poor. The reason for this phenomenon is that the generation of SERS effect is related to the enhancement of the local electromagnetic field on the surface of the substrate. Raman scattering does not require the change of dipole moment, but requires the change of polarizability. The laser wavelength used in the experiment is 532 nm, and due to high polarizability and relatively small impedance matching in the visible light range, Ag nanoparticles can enhance the local electromagnetic field of incident lights more effectively, thereby enhancing the SERS signals; and Ag nanoparticles are more prone to charge transfer than Au nanoparticles, this is due to the better conductivity of Ag, and charge transfer is also one of the important mechanisms of SERS signal enhancement. It can enhance the interaction between molecules and nanoparticles. Therefore, the charge transfer effect of the Ag nanoparticles on the porous silicon Bragg mirror substrate is stronger, thus the SERS performance is higher.

Therefore, it can be obtained that the AgNPs/CuNPs/Bragg-PSi SERS substrate has the most excellent SERS performance. The linear fitting between the negative logarithm of CV solution

concentration and the linear fitting degree of Raman peak intensity at 1617 cm^{-1} is as shown in Fig. 3(d). It can be seen that the intensity of the characteristic peak at 1617 cm^{-1} also decreases continuously during the process that the CV solution concentration decreases from 10^{-6} M to 10^{-11} M, which is in a linear relationship (R^2 = 0.9315), thus indicating that the substrate has certain accuracy for the detection on the CV solution concentration. However, due to the agglomeration of Ag nanoparticles on the surface of the substrate, the morphology and distribution are not very uniform, therefore there is still room for improvement in detection accuracy.

3.3 Optimization on soaking concentration of AgNPs/CuNPs/Bragg-PSi in $Cu(NO_3)_2$ solution

The performance of the SERS substrate is affected by many conditions. Ag nanoparticles have excellent SERS performance. The combination of Cu and Ag nanoparticles is selected because Cu nanoparticles have good electronic conductivity and rich surface active sites, which can provide more local electric field enhancement effects, thus increasing the strength of SERS signals. This is especially beneficial to SERS applications of detecting low-concentration molecules or enhancing weak signals, therefore, it is very important to study the influence of copper nitrate concentration on the performance of the SERS substrate by changing the immersion concentration of the copper nitrate solution. As shown in Fig. 4, in preparation of the AgNPs/CuNPs/Bragg-PSi substrate, the concentrations of copper nitrate are 0.1 M, 0.25 M, 0.5 M, 0.75 M and 1 M respectively, and the soaking time is 1 min; by comparing the SERS spectrum of 10^{-5} M CV solution (532 nm laser, 5% laser power, 3 s integration time, 3 integration times), because less Cu atoms are generated when the concentration is too low, the influence on the substrate is less; when the concentration is too high, agglomeration of CuNPs would be caused, and further the SERS performance of the substrate is influenced, so that the 0.75 M $Cu(NO_3)_2$ solution is the best choice; and due to the introduction of Cu nanoparticles and by virtue of adjusting the morphology and structure of the substrate and optimizing the distribution and arrangement of nanoparticles, the SERS effect is further enhanced.

3.4 Optimization of AgNPs/CuNPs/Bragg-PSi substrate by thermal annealing

The prepared AgNPs/CuNPs/Bragg-PSi SERS substrate was annealed respectively at 80 °C, 160 °C and 240 °C. As shown in Fig. 5(a), when the annealing temperature was 80 °C, arrangement of Ag nanoparticles began to get more homogenized, which was due to the fact that annealing made the Ag nanoparticles gradually begin to rearrange on the surface of the porous silicon Bragg substrate;[28] when the annealing temperature was 160 °C, as shown in Fig. 5(b), the agglomerated Ag nanoparticles began to break apart, high temperature made the Ag nanoparticles more active, as a result, the Ag nanoparticles were rearranged to form a more uniform spherical structure;[29] when the annealing temperature was 240 °C, as shown in Fig. 5(c), the fractured silver nanospheres clustered again, the spacing became larger, and high temperature made part of Ag nanoparticles break apart and reaggregate, which was due to the reason that surface diffusion and surface energy change caused by high temperature made the interaction of Ag nanoparticles change, the spacing among such reaggregated Ag nanoparticles became larger, and the SERS performance was reduced. SERS spectral characterizations were conducted on the AgNPs/CuNPs/Bragg-PSi substrates after annealing treatments at 80 °C, 160 °C, and 240 °C in a 10^{-5} M CV solution, as shown in Fig. 5(d). The results indicate that the AgNPs/CuNPs/Bragg-PSi substrate exhibits the most superior SERS performance at an annealing temperature of 160 °C. Fig. 5(e and f) respectively show the mapping image and EDS spectrum of the AgNPs/CuNPs/Bragg-PSi substrate at an annealing temperature of 160 °C. These images and spectrum reflect the distribution and proportion of Si, O, Cu, and Ag elements after the annealing treatment. Wherein the ratio of Cu elements to Ag elements was

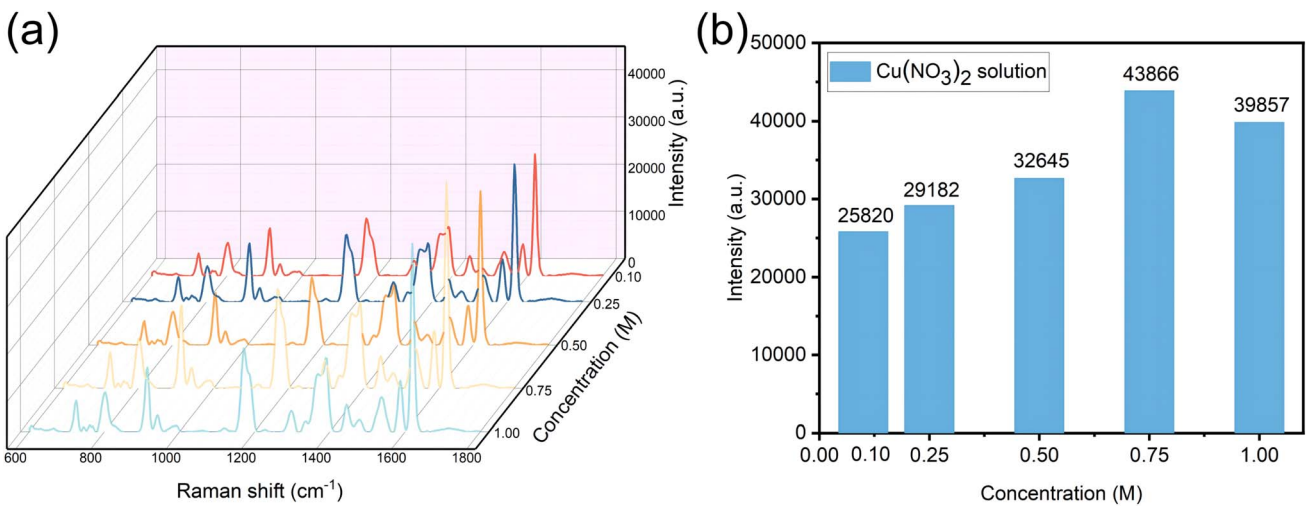

Fig. 4 (a) shows SERS spectra of 10^{-5} M CV solution soaked in different concentrations of $Cu(NO_3)_2$ solution; (b) shows the relationship between the concentration of $Cu(NO_3)_2$ solution and its Raman peak intensity at 1617 cm^{-1}.

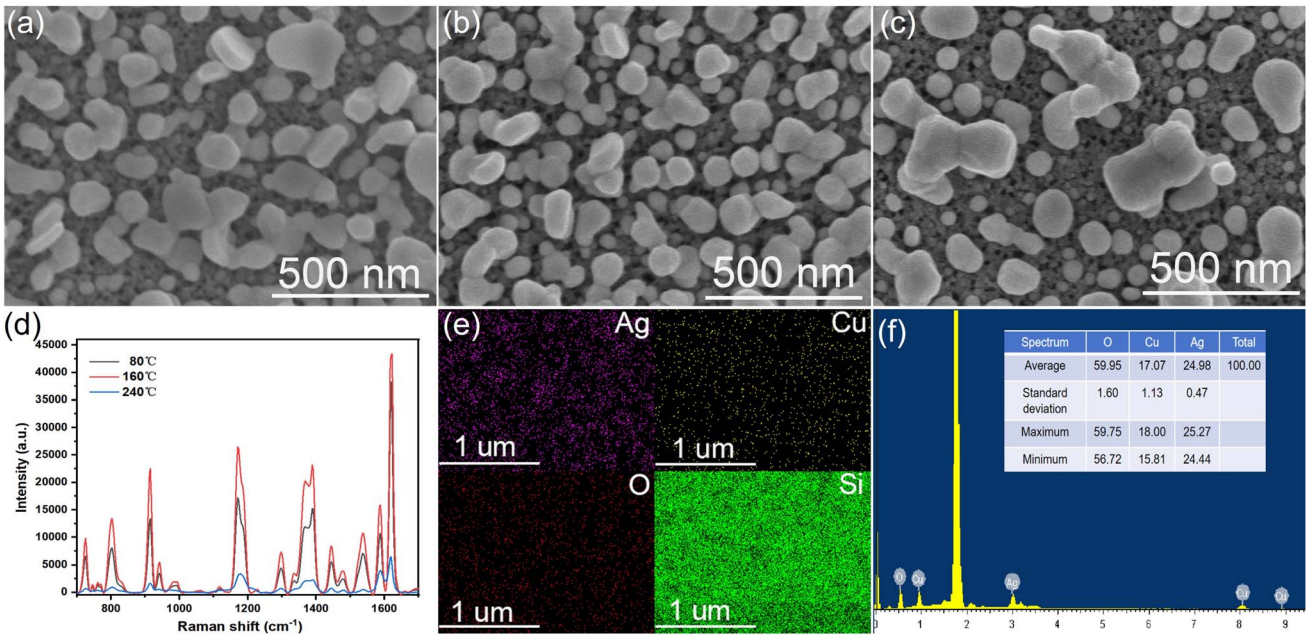

Fig. 5 (a–c) show SEM images of AgNPs/CuNPs/Bragg-PSi substrates annealed at 80 °C, 160 °C and 240 °C; (d) SERS spectra of AgNPs/CuNPs/Bragg-PSi substrates after annealing treatments at 80 °C, 160 °C, and 240 °C for 10^{-5} M CV solution; (e) mapping image of AgNPs/CuNPs/Bragg-PSi substrate after annealing at 160 °C; (f) shows EDS energy spectra of annealed AgNPs/CuNPs/Bragg-PSi substrates.

17.07 : 24.98, and the reason why Cu element content was less than Ag element content was that some CuNPs was used to replace AgNPs.

To further determine the elemental composition and valence states of the AgNPs/CuNPs/Bragg-PSi substrate, XPS testing was conducted, and the results are as follows. The high-resolution

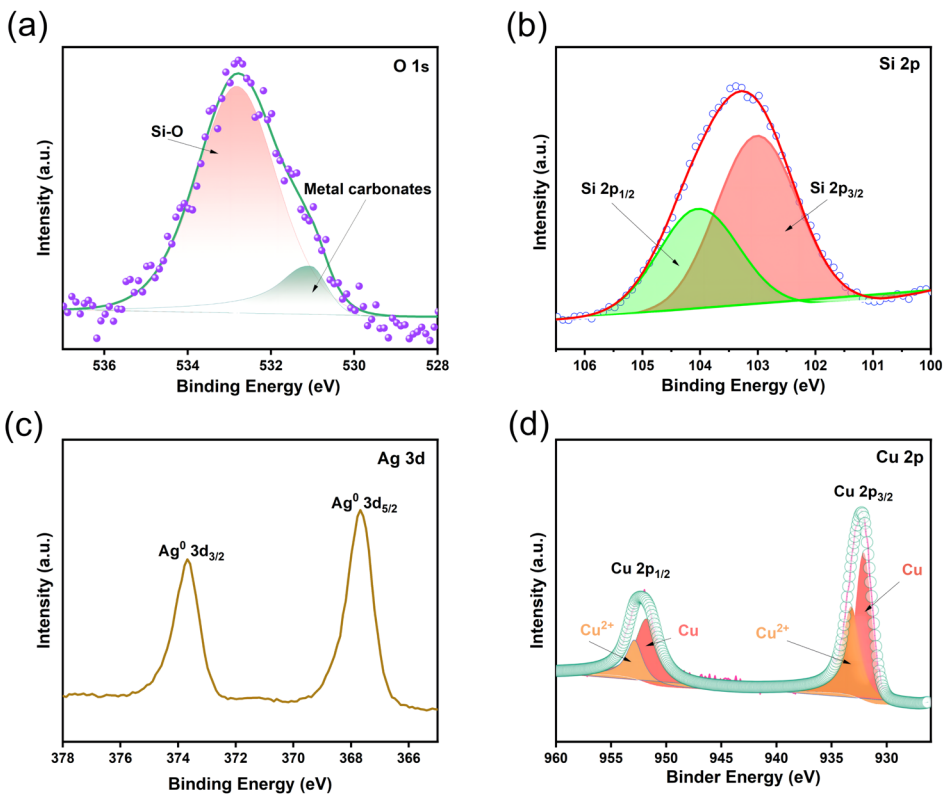

Fig. 6 XPS spectra of the AgNPs/CuNPs/Bragg-PSi substrate: (a) O element spectrum; (b) Si element spectrum; (c) Ag element spectrum; (d) Cu element spectrum.

spectrum of the O element (O 1s) is shown in Fig. 6(a), with peaks at binding energies of 532.78 eV and 531.08 eV corresponding to Si–O and metal oxide, respectively. Fig. 6(b) shows the high-resolution spectrum of Si 2p, with peaks at 103.98 eV and 102.98 eV corresponding to Si $2p_{1/2}$ and Si $2p_{3/2}$, respectively. Fig. 6(c) presents the high-resolution spectrum of Ag 3d, with peaks at binding energies of 373.68 eV and 367.68 eV corresponding to Ag^0 $3d_{3/2}$ and Ag^0 $3d_{5/2}$, respectively. Fig. 6(d) is the high-resolution spectrum of Cu 2p, with peaks at binding energies of 952.88 eV and 951.78 eV corresponding to Cu $2p_{1/2}$ for Cu^{2+} and Cu^0, and peaks at 933.28 eV and 932.08 eV corresponding to Cu $2p_{3/2}$ for Cu^{2+} and Cu^0, respectively. These results provide further evidence that AgNPs and CuNPs have been effectively loaded onto the Bragg-PSi substrate.

3.5 Measurement of substrate reproducibility and long-term stability

Reproducibility measurements and time-dynamics studies were conducted on the AgNPs/CuNPs/Bragg-PSi substrate, as shown in Fig. 7(a) and (b). Fifteen random control groups were selected for testing, and the average intensity of the 15 measurements was 35 124 (RSD = 2.7%). These experimental results indicate that the substrate has high reproducibility. The time-dynamics study results are presented in Fig. 7(c), showing that the SERS performance gradually decreases with increasing storage time. The decrease was not significant within the first week, but after one month, the SERS intensity was reduced by nearly half. This also demonstrates that the AgNPs/CuNPs/Bragg-PSi substrate has a certain degree of long-term stability, with good stability within one week. In summary, the prepared AgNPs/CuNPs/Bragg-PSi substrate exhibits high sensitivity, good reproducibility, and stability.

3.6 SERS detection of DPHP

The high-sensitivity AgNPs/CuNPs/Bragg-PSi SERS substrate was adopted to perform SERS spectrum detection on different concentrations of DPHP. In this experiment, acetone was used as a solvent, and the steps were as follows: soaking for 3 hours,

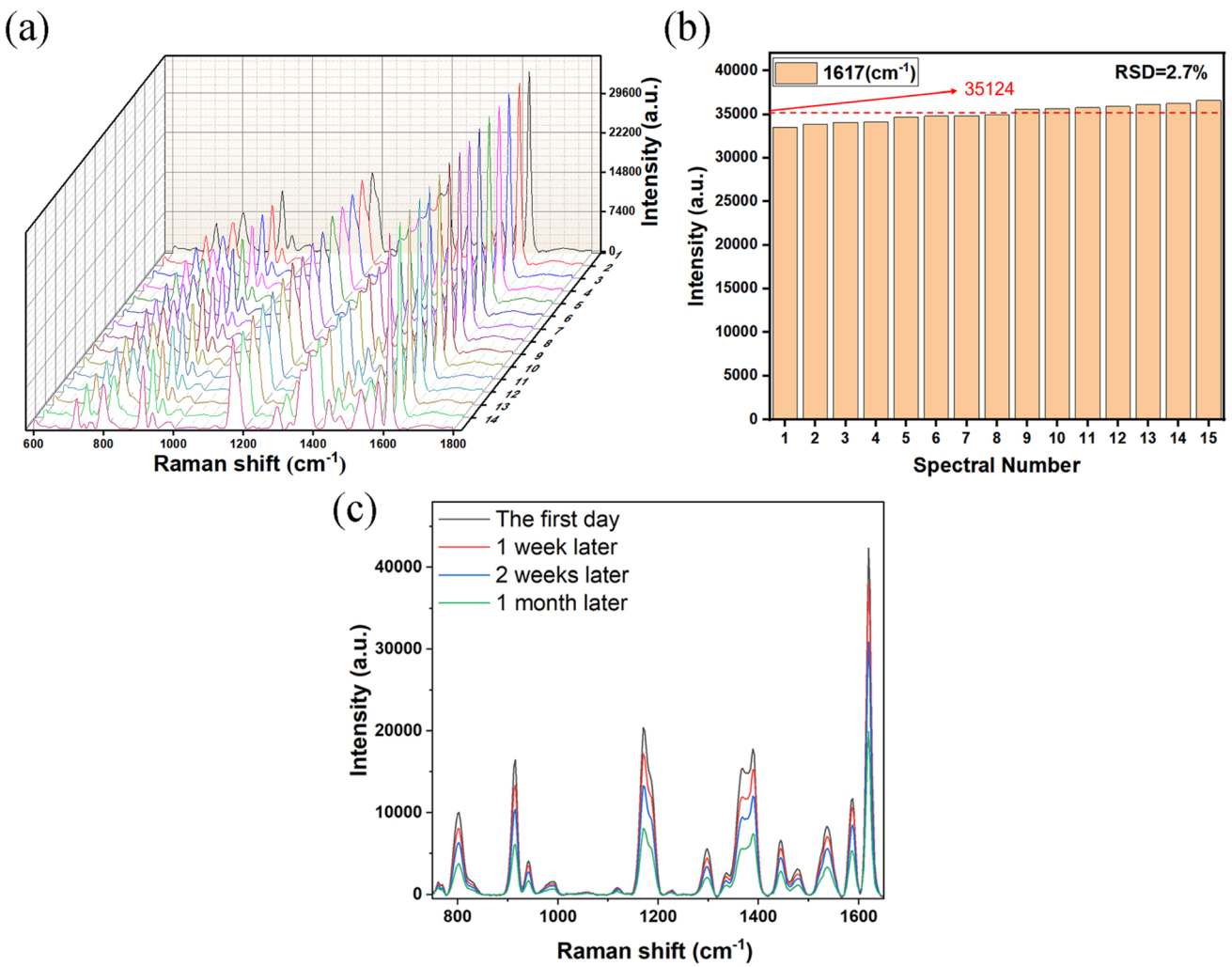

Fig. 7 (a) Randomly record the SERS spectra of 15 points of the CV solution; (b) the distribution of peak intensity at 1617 cm^{-1} for the SERS spectra of 15 randomly selected CV solutions, with the green line representing the average intensity; (c) the relationship between the SERS signal intensity of AgNPs/CuNPs/Bragg-PSi substrates and their storage time.

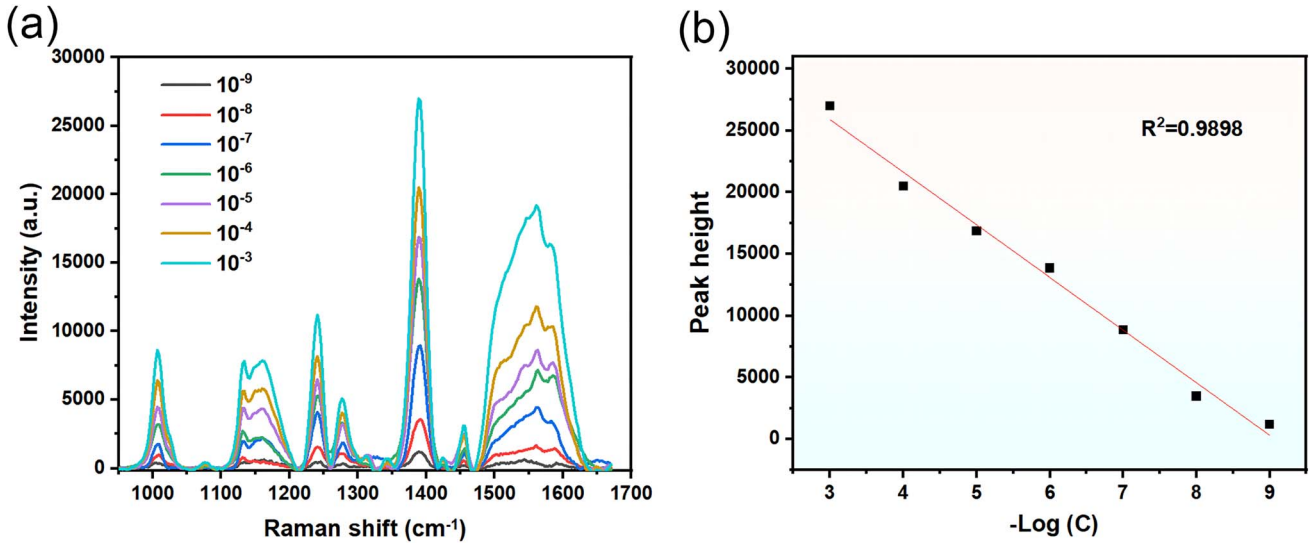

Fig. 8 (a) shows SERS spectrum of 10^{-3}–10^{-9} M diphenyl phthalate (DPHP); (b) shows linear fitting of the negative logarithm of the AgNPs/CuNPs/Bragg-PSi substrate to the DPHP solution concentration and its Raman peak intensity at 1388 cm^{-1}.

taking out and naturally drying the substrate for test; at 532 nm laser wavelength, setting the laser power as 50%, the integration time as 10 s and the integration times as 3 times; performing detailed analysis on the measured SERS spectrum; and determining the Raman frequency corresponding to the DPHP characteristic peak.

In the comparative analysis, several Raman peaks related to DPHP characteristic peaks were analyzed.[30] As shown in Fig. 8(a): 1009 cm^{-1} (ν(C=C) vibration), 1133 cm^{-1} (ν(O–C) vibration), 1240 cm^{-1} ($\gamma(CH_3)$ vibration), 1279 cm^{-1} (ν(C–O–C) vibration), 1388 cm^{-1} (δ(CH)/δ *sym*(CH_3)/δ(CCC) ring vibration), 1456 cm^{-1} (δ *sym*(CH_3) vibration) and 1563 cm^{-1} (ν(C=C)/γ (ring)/β (ring) vibration). It is particularly noteworthy that the Raman peak at 1388 cm^{-1} showed obvious height and sharpness. In order to evaluate the relationship between the DPHP concentration state and the SERS spectrum, this peak was selected as the characteristic peak of DPHP for further analysis. As shown in Fig. 8(b), linear fitting was performed between the negative logarithm of DPHP solution concentration and its Raman peak intensity at 1388 cm^{-1}, and the results showed that there was a good linear relationship ($R^2 = 0.9898$) between the two, which further verified that the SERS substrate has the characteristics of high sensitivity and strong accuracy and is capable of detecting the presence of DPHP.

Comparing the detection ranges of PAEs currently reported, as shown in Table 1, for the SERS detection of DEHP and DBP, the AuNP@PDA-MIP/rMoS_2/SPE and ZIFs-67@Ag NWs substrates exhibit lower detection limits. However, the AgNPs/CuNPs/Bragg-PSi substrate prepared in this study offers a more convenient, rapid, and cost-effective preparation method. The detection limit for DPHP in this study is 1×10^{-9} M, which can be converted to 0.31 ng mL^{-1} based on the molecular weight of DPHP (318.32). Compared to other detection methods, SERS spectroscopy can save more time and also has a broader detection range and extremely low detection limit.

Table 1 Comparison of the currently reported PAEs detection ranges

Substance	Method	Detection range
DEHP[30]	SERS	$\geq 2.3 \times 10^{-11}$ M
DNPP[31]	MSPE & HPLC	0.1–600 μg L^{-1}
Phthalates[32]	UPLC-ESI-MS/MS	0.5–50 ng mL^{-1}
BBP[14]	ELISA	2.5–2566.3 ng mL^{-1}
DBP[33]	SERS	10^{-2}–10^{-12} mol L^{-1}
PHP[34]	SERS	$\geq 10^{-9}$ mol L^{-1}
DIBP[35]	CL-ELISA	5.0–170.8 ng mL^{-1}

In summary, this study has successfully realized SERS detection on DPHP with different concentrations based on the high-sensitivity AgNPs/CuNPs/Bragg-PSi SERS substrate. The characteristic peak of the substrate at 1388 cm^{-1} provided accurate and sensitive analysis results with detectable concentrations ranging from 10^{-3} M to 10^{-9} M, which further demonstrated the excellent performance of the SERS substrate in detecting DPHP molecules, indicating that the technology can be used for qualitative and quantitative detection at ultra-low concentrations.

4 Conclusions

This study has successfully prepared the AgNPs/CuNPs/Bragg-PSi substrate and estimated its performance in detecting the CV solution and DPHP. Experimental results show that the porous silicon substrate prepared by use of the electrochemical etching method is capable of effectively providing more SERS active sites, thus realizing high-sensitivity detection on specific molecules. By virtue of introducing Ag and Cu nanoparticles onto the porous silicon substrate, the SERS performance of the substrate is obviously enhanced; especially in the AgNPs/CuNPs/Bragg-PSi substrate, combination

of the Ag nanoparticles and Cu nanoparticles can provide more local electric field enhancement effects, and the SERS signal strength is furthermore increased. In comparison with other substrates, the AgNPs/CuNPs/Bragg-PSi substrate has better SERS performance and detection sensitivity. In addition, the proper annealing temperature can improve the arrangement of Ag nanoparticles on the substrate and enhance the stability and consistency of signals. This study has successfully developed the AgNPs/CuNPs/Bragg-PSi substrate with excellent SERS performance and made preliminary verification on its application potential in molecular detection. These results provide a new possibility for the application of the SERS technology in biomedicine, environmental monitoring and other fields, and lay a foundation for further research and development of high-performance SERS substrates.

Data availability

All data used in this study are available upon reasonable request. If you wish to obtain the data, please contact the author at [2497102698@qq.com]. We will provide the requested data as soon as possible upon receiving the request.

Author contributions

Bowen Sun (first author): methodology, validation, formal analysis, investigation, data curation, writing – original draft, writing – review and editing, visualization. Peng Li (corresponding author): conceptualization, methodology, formal analysis, investigation, validation, writing – review and editing, supervision, resources, funding acquisition, project administration. Shuguo Yu: visualization, supervision, project administration, writing – review and editing. Xiaohui Huang: software, supervision, project administration, writing – review and editing. Liangjun Ma: investigation, writing – review and editing.

Conflicts of interest

There are no conflicts to declare.

Acknowledgements

This work was supported by Xinjiang Uygur Autonomous Region Natural Science Foundation (2022D01C49).

Notes and references

1 Y. Wu, J. Sun, C. Zheng, X. Zhang, A. Zhang and H. Qi, *Environ. Sci. Pollut. Res.*, 2019, **26**, 11224–11233.
2 K. Li, D. Ma, J. Wu, C. Chai and Y. Shi, *Chemosphere*, 2016, **164**, 314–321.
3 J. Sun, L. Pan, Y. Zhan, H. Lu, D. C. Tsang, W. Liu, X. Wang, X. Li and L. Zhu, *Sci. Total Environ.*, 2016, **544**, 670–676.
4 M. Bi, W. Liu, X. Luan, M. Li, M. Liu, W. Liu and Z. Cui, *Environ. Sci. Technol.*, 2021, **55**, 13980–13989.
5 Y. Zhang, Y. Yang, Y. Tao, X. Guo, Y. Cui and Z. Li, *J. Hazard. Mater.*, 2023, 132182.
6 J. Pan, P. Liu, X. Yu, Z. Zhang and J. Liu, *Front. Endocrinol.*, 2024, **14**, 1324993.
7 H. Hlisníková, I. Petrovičová, B. Kolena, M. Šidlovská and A. Sirotkin, *Pharmacol. Rep.*, 2021, **73**, 386–404.
8 W.-H. Chang, S. Herianto, C.-C. Lee, H. Hung and H.-L. Chen, *Sci. Total Environ.*, 2021, **786**, 147371.
9 S. Benjamin, E. Masai, N. Kamimura, K. Takahashi, R. C. Anderson and P. A. Faisal, *J. Hazard Mater.*, 2017, **340**, 360–383.
10 L. Niu, Y. Xu, C. Xu, L. Yun and W. Liu, *Environ. Pollut.*, 2014, **195**, 16–23.
11 N. A. Ayofe, P. O. Oladoye and D. O. Jegede, *Chem. Int.*, 2018, **4**, 85.
12 A. Dan, S. Zhang, Z. Chen, J. Dong, W. Zheng, Y. Tu, Z. Lin and Z. Cai, *Talanta*, 2023, **253**, 123923.
13 M. V. Russo, P. Avino, L. Perugini and I. Notardonato, *RSC Adv.*, 2015, **5**, 37023–37043.
14 M. Li, Y. Cui, Z. Liu, Y. Xue, R. Zhao, Y. Li and D. Du, *Sci. Total Environ.*, 2019, **687**, 849–857.
15 N. Zhu, X. Li, Y. Liu, J. Liu, Y. Wang, X. Wu and Z. Zhang, *Sci. Total Environ.*, 2021, **784**, 147212.
16 B. Sharma, R. R. Frontiera, A.-I. Henry, E. Ringe and R. P. Van Duyne, *Mater. Today*, 2012, **15**, 16–25.
17 S. E. Bell, G. Charron, E. Cortés, J. Kneipp, M. L. de la Chapelle, J. Langer, M. Procházka, V. Tran and S. Schlücker, *Angew. Chem., Int. Ed.*, 2020, **59**, 5454–5462.
18 H. Liu, X. Gao, C. Xu and D. Liu, *Theranostics*, 2022, **12**, 1870.
19 T. Gong, C. M. Das, M.-J. Yin, T.-R. Lv, N. M. Singh, A. M. Soehartono, G. Singh, Q.-F. An and K.-T. Yong, *Coord. Chem. Rev.*, 2022, **470**, 214711.
20 J. Perumal, Y. Wang, A. B. E. Attia, U. Dinish and M. Olivo, *Nanoscale*, 2021, **13**, 553–580.
21 T. Itoh, M. Procházka, Z.-C. Dong, W. Ji, Y. S. Yamamoto, Y. Zhang and Y. Ozaki, *Chem. Rev.*, 2023, **123**, 1552–1634.
22 J. Wang, Z. Jia and Y. Liu, *IEEE Sensor. J.*, 2019, **19**, 11221–11227.
23 V.-T. Vo, V.-D. Phung and S.-W. Lee, *Surface. Interfac.*, 2021, **25**, 101181.
24 B. P. Nanda, P. Rani, P. Paul, R. Bhatia, *et al.*, *Int. J. Pharm. Anal.*, 2024, **14**(11), 100959.
25 S. Han, C. Chen, C. Chen, L. Wu, X. Wu, C. Lu, X. Zhang, P. Chao, X. Lv, Z. Jia, *et al.*, *Anal. Chim. Acta*, 2023, **1254**, 341116.
26 D. Xu, Y. Zhang, S. Zhang, W. Yang, Z. Wang and J. Li, *Opt Laser. Technol.*, 2022, **145**, 107502.
27 L. He, C. Liu, J. Tang, Y. Zhou, H. Yang, R. Liu and J. Hu, *Appl. Surf. Sci.*, 2018, **434**, 265–272.
28 H. Sun, X. Lian, Y. Lv, Y. Liu, C. Xu, J. Dai, Y. Wu and G. Wang, *Materials*, 2020, **13**, 4205.
29 A. Bonyár, I. Csarnovics, M. Veres, L. Himics, A. Csik, J. Kámán, L. Balázs and S. Kökényesi, *Sens. Actuators, B*, 2018, **255**, 433–439.
30 Y. Yang, Y. Li, W. Zhai, X. Li, D. Li, H. Lin and S. Han, *Anal. Chem.*, 2020, **93**, 946–955.

31 Y. Wu, Q. Zhou, Y. Yuan, H. Wang, Y. Tong, Y. Zhan, X. Sheng, Y. Sun and X. Zhou, *Talanta*, 2020, **206**, 120213.
32 W. Li and J. Duan, *Anal. Methods*, 2011, **3**, 314–321.
33 H. Xu, J. Zhu, X. Wu, Y. Cheng, D. Wang and D. Cai, *Spectrochim. Acta, Part A*, 2023, **284**, 121735.
34 H. Wang, C. Wang, J. Huang, Y. Liu, Y. Wu, R. You, J.-H. Zhang, Y. Lu and H. Shen, *Food Chem.*, 2023, **409**, 135363.
35 A. N. Berlina, M. Y. Ragozina, D. I. Gusev, A. V. Zherdev and B. B. Dzantiev, *Chemosensors*, 2023, **11**, 393.